JES Focus Issue on Redox Flow Batteries—Reversible Fuel Cells

In Situ Localized Current Distribution Measurements in All-Vanadium Redox Flow Batteries

Jason T. Clement,* Douglas S. Aaron, and Matthew M. Mench,z**

Department of Mechanical, Aerospace, and Biomedical Engineering, University of Tennessee, Knoxville, Tennessee 37996, USA

A printed circuit board (PCB) was implemented for in-plane, two-dimensional distributed current measurements in an all-vanadium redox flow battery (VRFB). A PCB with built-in shunt resistors is a passive method of measuring localized currents in-situ, in real time. It is demonstrated that lateral current spread through non- or partially-segmented flow field plates will produce a distribution that does not properly reflect the distribution within the electrode; this issue is resolved in this work via fully-segmented flow plates. Large current gradients develop when a cell reaches a mass-transport limitation. Based upon the resultant distributions, it is shown that they reflect a combination of electrolyte velocity and local concentration within the electrode. The impact of flow rate and electrode material properties such as wettability, surface area, porosity, and thickness on current distribution are presented.

Manuscript submitted August 19, 2015; revised manuscript received October 28, 2015. Published November 24, 2015. *This paper is part of the JES Focus Issue on Redox Flow Batteries–Reversible Fuel Cells.*

Redox flow batteries (RFBs) are electrochemical energy storage devices that have received much attention in recent years for their capabilities as grid-scale energy storage.[1] Comprised of a battery stack and externally-stored liquid electrolyte, these systems provide the advantage of decoupled power and energy capacity. Compared to other large-scale energy storage options such as pumped hydro or compressed air storage, these systems have a small footprint and no geographic limitations.[2] These aspects make RFBs an attractive storage system to complement renewable energy sources and potentially cover base-load power needs.

Another attractive aspect of these systems is the flexibility of the electro-active species. RFBs operate on coupled redox reactions at electrodes separated by an ion exchange separator. This provides countless options for different chemistries, some of the most common include all-vanadium, vanadium/bromine, bromine/polysulfide, and iron/chromium, among others.[3] The all-vanadium chemistry, in particular, utilizes the four stable oxidation states of the transition metal to store electrical energy. This is an attractive choice because the same active species on both half-cells allows the liquid electrolytes to be rebalanced to regain capacity loss due to self-discharge.

Published research on these systems has resulted in improved individual cell components such as membranes,[4,5] electrodes,[6,7] and electrolyte.[8,9] In addition, investigations of flow field design[10,11] and operating conditions[12,13] have improved transport, performance, and efficiency of operating cells. However, these improvements are typically quantified with ex-situ experiments, or are validated with an overall cell performance comparison. Ex-situ experiments, while useful, do not always translate directly to an operating cell. On the other hand, performance of an operating cell only provides an overall cell average; thus, any local changes would be undetectable. Localized real-time knowledge of performance within cells can enable insight into optimization of architecture, materials, charging, discharging, operational transients, or other aspects that can further extend longevity and enhance performance. Additionally, localized measurements can be used for highly detailed model validation that is not possible with whole-cell performance measurements.

For these reasons, distributed diagnostic techniques are advantageous to probe localized behavior. At the time of writing, two such techniques have been applied to a vanadium redox flow battery (VRFB): through-plane potential distribution, and in-plane current distribution.[14–16] Liu et al. showed with potential distribution measurements that with increasing current density, the reaction location localizes toward the flow plate.[14]

In-plane current distribution measurements have been extensively studied in fuel cells.[17] There are three primary approaches for localized current measurements in electrochemical cells: hall sensors,[18,19] shunt resistors,[20,21] or printed circuit boards.[22,23] Hall sensors operate by measuring the magnetic induction of the magnetic field surrounding an electric current.[18] The shunt resistor and PCB techniques operate on the same principle by measuring voltage drop across a resistor; however the PCB approach is more advantageous, which will be discussed. The implementation of current distribution measurements is easily translated from fuel cells to flow batteries because of the similarities in cell architecture.[24]

Only one other published study to date has examined in-plane current density distribution measurements in VRFBs.[16] However, this study is distinctly different in several ways; the two most important differences include cell architecture and measurement technique. Hsieh and coworkers used a traditional flow frame cell design, whereas this work utilizes a flow channel architecture with a serpentine design.[16,24] The terms "flow frame" and "flow channel" are used here to describe the architecture, contrary to the more commonly used "flow-through" and "flow-by," which imply the governing electrolyte transport mechanism into the electrode: convection, and diffusion, respectively. According to these definitions, a serpentine flow channel would be considered a "flow-by" whereas an interdigitated flow channel would be considered "flow-through." However, these terms are slightly misleading because modeling efforts have shown that, in a serpentine design, electrolyte bypasses the channel and passes through the electrode at the channel switchbacks.[25] In fact, the average velocity through the electrode layer is higher with serpentine than interdigitated.[25] Therefore, this architecture should not be considered a true "flow-by," as the term implies there is minimal convective transport through the electrode. These observations will depend on the specific cell design; however, the referenced work studied the same design, making this a relevant finding.

Hsieh and coworkers studied two different types of cell segmentation: one with a segmented current collector and one with a segmented flow plate.[16] The segmented current collector design had poor compression and was subjected to lateral current spread through the flow plate, thus causing inaccurate current measurements. This lateral spread has also been observed in previous work with a PCB approach

*Electrochemical Society Student Member.
**Electrochemical Society Active Member.
zE-mail: mmench@utk.edu

and partially-segmented flow plate.[15] Eckl et al. modeled lateral current spread for fuel cell current distribution measurements and found that, without segmented plates, current spread can be significant.[26] The second cell used by Hsieh et al. had a fully-segmented flow plate, which eliminated lateral current spread, however, it suffered from lower voltage efficiency and discharge capacity.[16] They attributed the performance decline to poor compression and high contact resistance between graphite segments and electrical connectors.

Fully-segmented plates are necessary to ensure accuracy with these measurements, however, there are two distinct approaches to manufacture them: machining from a single block of conductive flow plate, or embedding conductive blocks within a non-conductive frame.[17] The latter suffers from compression issues because the plate is made of two different materials, which makes proper sizing and even compression difficult. For those reasons, manufacturing from a single block is more advantageous.

In addition to the segmentation method, measurement technique strongly impacts the accuracy of distributed current measurement. Hsieh et al. used a series of shunt resistors hard-wired into the cell, and as a result, their cells suffered from added contact resistance between the segments and measurement system.[16] A PCB, however, eliminates these issues because electrical connections are made within the PCB, which is evenly compressed within the cell. Internal connections with the PCB approach also promote higher spatial resolution because the minimum segment size is then dictated by the practical limitations of machining a flow field. The resolution of a hard-wired network, on the other hand, is restricted by the diagnostic itself and the size constraints of the interface connections between the flow plate and resistors. Each segment in this work, for example, is 1/16 the area of those used by Hsieh and coworkers.[16] Spatial resolution is important for drawing correlations between current and electrolyte transport within the cell.

In addition, the PCB is independent of the cell, which allows for easy replacement of the flow field plate to examine different flow channel designs. A PCB also has the capability of being implemented between cells in a stack, which would be more difficult or impossible with some other techniques. These aspects indicate that the use of a PCB is more advantageous than a hard-wired resistor network.

There is a lack of in-situ diagnostics for VRFBs, so correlations between distributed data and transport are not yet fully understood. The scope of this work is to implement and validate the PCB approach as an accurate diagnostic for in-plane localized current density measurements in a laboratory-scale VRFB. This initial study investigates of the influence of flow rate, operating conditions, and electrode materials on resulting current distributions. It is verified that these measurements reflect a combination of mass transport and electrolyte concentration gradients across the cell active area.

Experimental

PCB and data acquisition.— In this setup, an 857 Redox Cell Test System potentiostat (Scribner Associates, Inc.) was used to control cell current and record high frequency resistance (HFR) measurements at a frequency of 10 kilohertz. Simultaneously, a National Instruments LabVIEW data acquisition system was used to passively collect data from the PCB in real time. The PCB is divided into 4.5 mm by 4.5 mm segments with 0.5 mm spacing, and was placed between the flow plate and current collector, as shown in Figure 1. Small pieces of SGL 10AA carbon paper (SGL Group) were inserted and compressed between the segments and flow plate to ensure good electrical contact. HFR measurements for the cell with and without the PCB were comparable, thus contact resistance between the PCB and flow plate used for testing was considered negligible. Current was collected at each segment where it passed through a shunt resistor; then all segments were combined on the opposite side of the PCB where the current passed to a gold-plated current collector, as shown in Figure 1.

Data were collected in 1 second intervals and averaged over 3 seconds. Averaged data are presented in one of three ways: raw data in grid format as measured directly by the data acquisition system, processed data via interpolation presented as a smoothed current density contour plot, or processed data illustrated as a percent deviation from the average current across the distribution. To process deviation distributions, current measurements from each segment for a given distribution were averaged; then each segment was compared to that average. This normalizes the data for comparison across various current densities and conditions.

Cell architecture.— The experimental setup consisted of a 9 cm^2 single cell VRFB with a serpentine flow channel architecture.[24] In order to accommodate the PCB between the flow plate and current collector, electrolyte was fed through the side of the flow plates, as shown in Figure 1. This work included one improvement upon the previous design: the use of fully-segmented flow plates. Flow plates were fabricated in-house from graphite composite BMC 940 (Bulk Molding Compounds, Inc.) following the same procedure that has been used for fuel cells.[27,28] Fully-segmented plates were made by machining channels to mirror the spacing on the PCB. These channels were then filled with a thermoset resin (EpoMet, Buehler) barrier that penetrated the entire thickness of the plate. The flow channel and inlet/outlet holes were then added to the segmented plate.

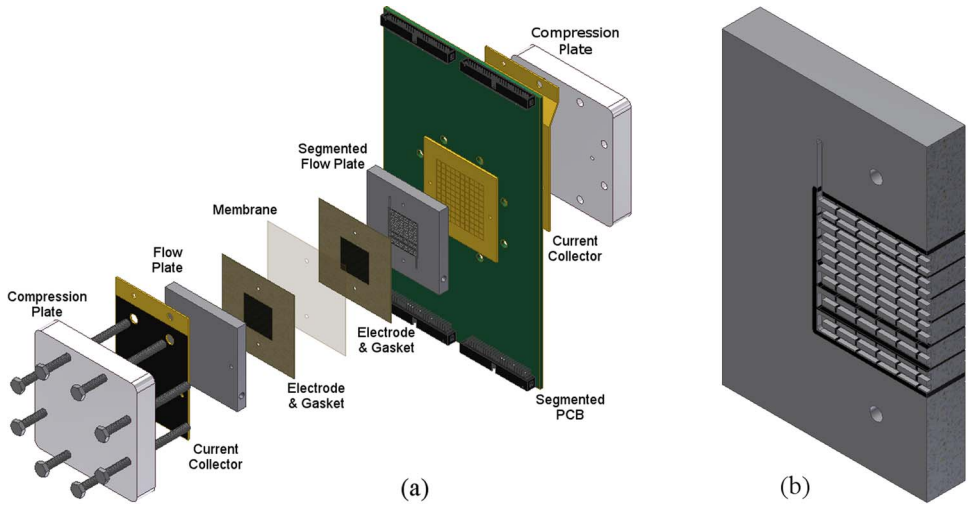

Figure 1. (a) Exploded view of the VRFB cell with PCB current distribution board and (b) cross-section view of a fully-segmented flow plate (black represents thermoset resin).

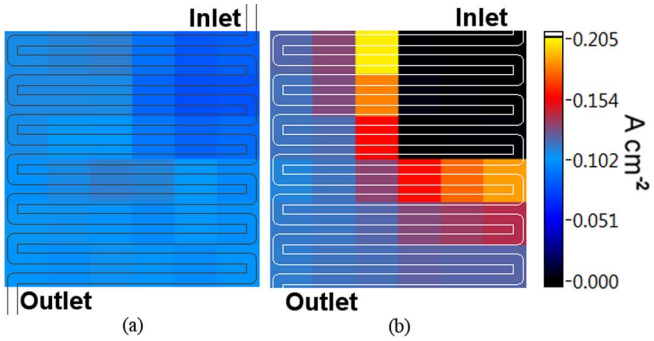

Figure 2. Impact of upper-right quadrant isolation on current distribution for (a) partially-segmented, and (b) fully-segmented flow plates during the plateau region of a 100 mA cm^{-2} discharge curve at a flow rate of 50 mL min^{-1}.

Full segmentation was deemed necessary since current can spread laterally within a partially-segmented flow plate.[15,26] This spread artificially dampens current gradients across the active area; thus, measured distributions are not an accurate representation of the distribution generated within the cell. In order to quantify this lateral spread, a portion of the active area was isolated with an electrical insulator between the electrode and flow plate, as explained elsewhere.[15] When applied to a fully-segmented cell, no current is measured in the isolated area, as expected. Figure 2 depicts this result with a comparison of the two flow plate types during a constant current discharge at 100 mA cm^{-2}. This indicates that fully-segmented plates transmit current with no spread between the electrode and PCB.

An additional outcome of this test is insight regarding current spread through the electrolyte. The isolated section covers the inlet channel, which electrolyte must pass through while in contact with multiple isolated segments. Since no current is measured in the isolated segments, current spread through the electrolyte in the channel is also determined to be negligible. Considering the relative lateral and through-plane length scales, this is expected. It should be noted that if there was a large potential gradient between segments there would presumably be some current spread through the electrolyte, similar to shunt currents in a stack with potential gradients between cells.[29]

Since the PCB was placed between the flow plate and current collector on one side of the cell, it was important to consider from which half-cell to measure the distribution. To verify that either side could be used with the same results, a series of comparison tests were conducted. Single-pass polarization curves were performed with the same cell build, the only difference being which electrolyte flowed through the PCB side of the cell. The two configurations had comparable performance and distributions under a limiting current condition, as shown in Figure 3. Thus, it was concluded that PCB placement did not impact the distributed current measurement. Since the PCB is essentially a small ohmic resistance in series with the electrodes, the only performance impact anticipated would be in the overall cell resistance. HFR measurements between these two configurations varied less than 3%. For all distributions shown hereafter, the PCB was placed on the negative half-cell.

Electrolyte preparation and testing procedures.— All cells were assembled with Nafion 117 (DuPont) membranes pretreated according to the procedure described elsewhere.[30] All tests were conducted with 1 mole dm^{-3} vanadyl sulfate (Alfa Aesar) with 5 mole dm^{-3} sulfuric acid (Alfa Aesar) electrolyte. Initially, the positive electrolyte volume was double that of the negative electrolyte; the VRFB was charged at 1.7 volts until a cutoff current of 30 mA was reached. Half of the positive electrolyte was then removed, resulting in identical volumes of fully-charged electrolyte. Electrolyte was remixed between tests and recharged to the same cutoff current. The electrolyte flow rate was 20 mL min^{-1} for all tests unless otherwise noted. Three different electrodes were used: untreated (as-received from the manufacturer) 10AA carbon paper (SGL Group), with a nominal thickness of 0.39 mm, treated 10AA carbon paper (SGL Group) that was heat treated in 42% oxygen environment at 400°C for 30 hours,[31] and untreated GFD3 carbon felt (SGL Group) with a nominal thickness of 3 mm. Electrodes were compressed to 75% of original thickness unless otherwise noted. All cells were compressed with bolts torqued to 10 newton-meters. Single-pass polarization curves were performed at a constant flow rate to ensure that a constant state of charge (SoC) was maintained throughout the entire duration of a test.

Results and Discussion

Typically, RFBs are evaluated through overall cell performance such as charge-discharge curves; however, distributed current diagnostics provide additional resolution of localized performance within the cell. This is useful for drawing correlations between performance and transport through these cells. A constant current discharge curve was performed to observe changes in distribution as the cell voltage changed along the curve, as shown in Figure 4. Towards the beginning of discharge a nearly uniform distribution was observed and persisted throughout the majority of the discharge curve. This type of distribution is desirable because it indicates sufficient delivery of electrolyte uniformly across the active area to maintain the reaction. However, as the concentration of active species is depleted, the voltage begins to drop off rapidly and large gradients begin to develop in the distribution. These gradients continue to develop until the cutoff voltage is reached indicating a limiting condition where the cell can no longer maintain the desired current. One limitation of a constant current discharge curve is that there is no delineation of the sources of overpotential that dominate voltage loss. A polarization curve, however, can offer insight into the different losses to some extent.

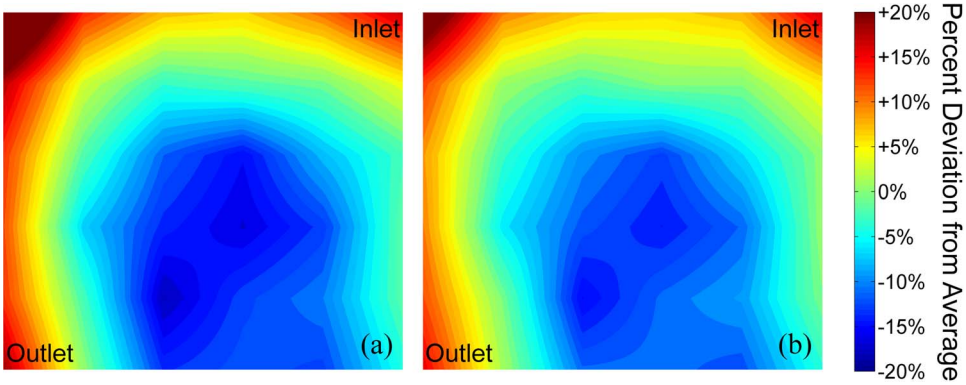

Figure 3. Current distribution comparison from 50% SoC single-pass polarization curves of untreated carbon paper electrode at limiting current (300 mA cm^{-2}) with the PCB on the (a) positive half-cell, and (b) negative half-cell.

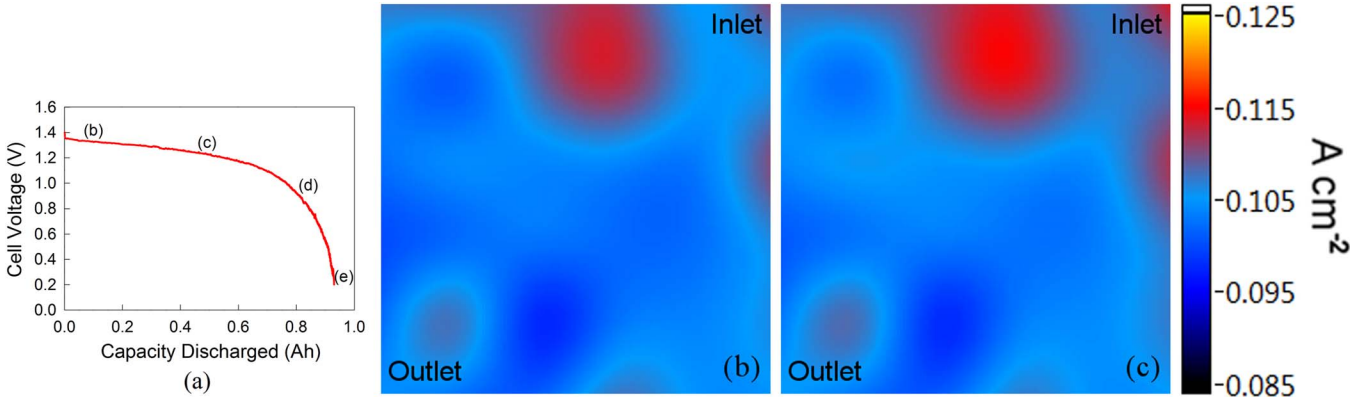

Figure 4. (a) Constant current discharge for an untreated carbon paper electrode at 100 mA cm^{-2} and corresponding current distributions at various points along the curve corresponding to (b) 75% SoC, (c) 50% SoC, (d) 25% SoC, and (e) 17% SoC.

A single-pass polarization curve (i.e. once electrolyte passes through the cell it is not recycled back for a second pass) at a constant flow rate delivers electrolyte at a constant SoC to the cell. This curve can then be separated into three regions in which the cell overpotential is dominated by a particular type of loss.[32] At low and moderate current densities, where the curve appears linear, losses are dominated by kinetic and ohmic overpotentials. However, mass transport losses can dominate overpotential at high currents. Figure 5 shows a single-pass polarization curve and corresponding current distributions at various points along the curve. The first three distributions of Figure 5 (5b, 5c, and 5d) correspond to locations of kinetic and ohmic-dominated losses. These data show very little distribution variation across the active area, which is similar to the beginning and plateau region of the constant current discharge curve. However, once the cell reached the mass transport limiting region, shown in Figures 5e and 5f, significant current gradients occurred. Under such conditions there is high reactant utilization (e.g. a cell with 75% SoC inlet, operating at 550 mA cm^{-2} has a SoC of 60% at the outlet).

The unique concave down shape of these current distributions can be correlated to convective transport within the cell. Computational fluid dynamic modeling of transport within this architecture has shown that, for a serpentine flow channel, there is significant convective transport of electrolyte through the electrode along the sides of the active area at the switchbacks of the channel.[25] Electrolyte bypasses the interior channels and jumps through the electrode as a result of a lower pressure drop through the electrode across the land compared to through the channel around the meander. Thus the distribution, under mass-transport limiting conditions, reflects the combination of transport coupled with the concentration gradient due to depletion from inlet to outlet. This finding highlights the advantage of this diagnostic technique: the ability to identify limitations with specific cell designs, operating conditions, and electrode materials.

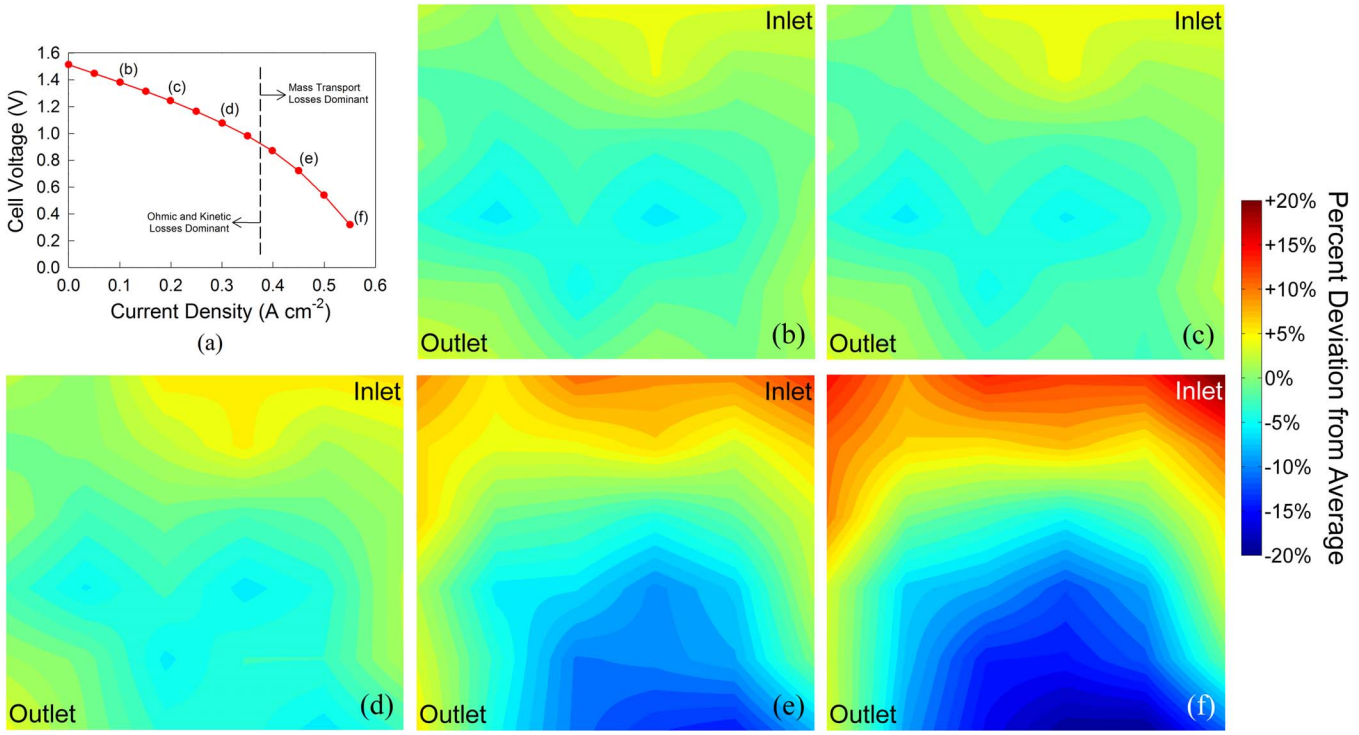

Figure 5. (a) Single-pass polarization curve for heat treated carbon paper at 75% SoC and corresponding current distributions at (b) 100 mA cm^{-2}, (c) 200 mA cm^{-2}, (d) 300 mA cm^{-2}, (e) 450 mA cm^{-2}, and (f) 550 mA cm^{-2}.

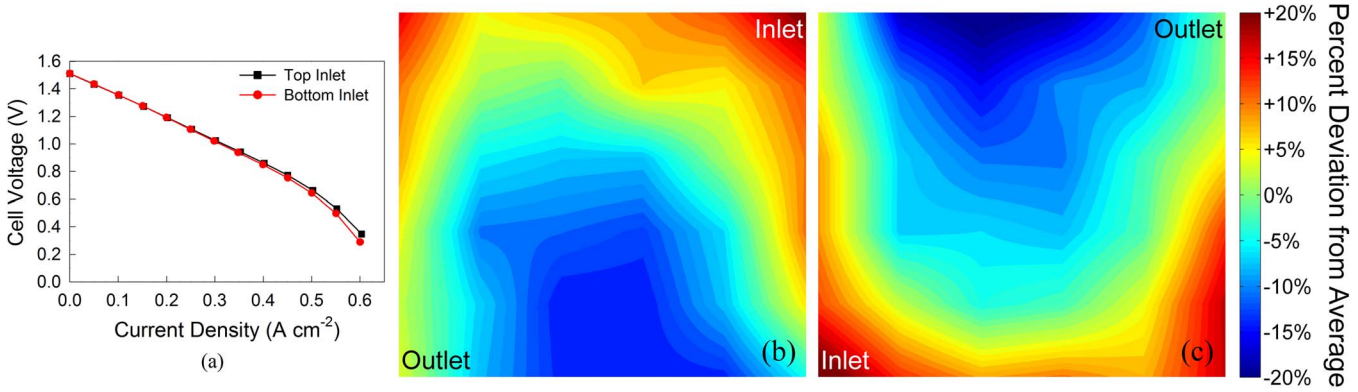

Figure 6. (a) Single-pass polarization curve comparison of an untreated carbon paper electrode at 75% SoC and corresponding current distributions at 600 mA cm^{-2} for (b) top inlet and (c) bottom inlet.

This behavior was also evident when the inlet location was reversed; Figure 6 compares distributions between a top-inlet fed cell with that of a bottom-inlet fed cell. Clearly, the high current region flipped between cases, yet the higher current along the edges of the cell was still present. This supports the assertion that in this system, current distributions closely mirror fluid transport in the electrode and electrolyte concentration gradients. Thus, the observed distributions are not simply a result of a non-uniform electrode or uneven compression on the cell. Uniform compression was verified using compression paper between each layer of the cell in an ex-situ cell assembly.

Current distributions also provide insight during constant current charging processes. For a single-pass, charging polarization curve at 50% SoC, shown in Figure 7, it is evident that the distributions are roughly the same, regardless of charging current. The maximum attainable charging current density is significantly lower than what is achievable during discharge (for the same SoC and flow rate) because charging is restricted by the electrochemical reactions for the redox couple. In this case the cell was limited to 1.8 V in order to prevent undesirable gas generation from side reactions.[33] The relatively uniform distributions indicate that charging is not a mass transport limited process; rather, it is limited by the electrochemical operating window of the cell redox couple. This was the case for other electrode materials and states of charge tested in this study, and holds true under typical VRFB operating conditions. It is possible to reach a mass transport limitation during charging, however only at unfavorable operating conditions of very high SoC and very low flow rate. For example, a cell with heat treated carbon paper electrodes reached a mass transport limited charging current

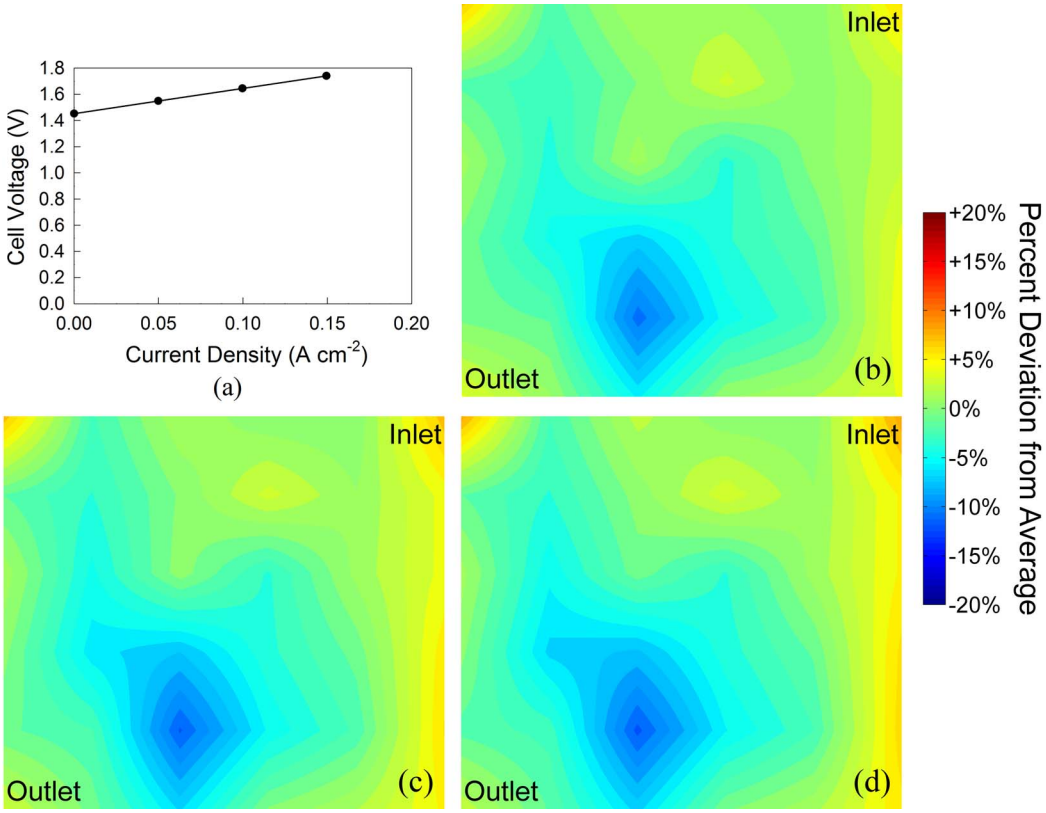

Figure 7. (a) Single-pass charging polarization curve for an untreated carbon paper electrode at 50% SoC and corresponding current distributions: (b) 50 mA cm^{-2}, (c) 100 mA cm^{-2}, and (d) 150 mA cm^{-2}.

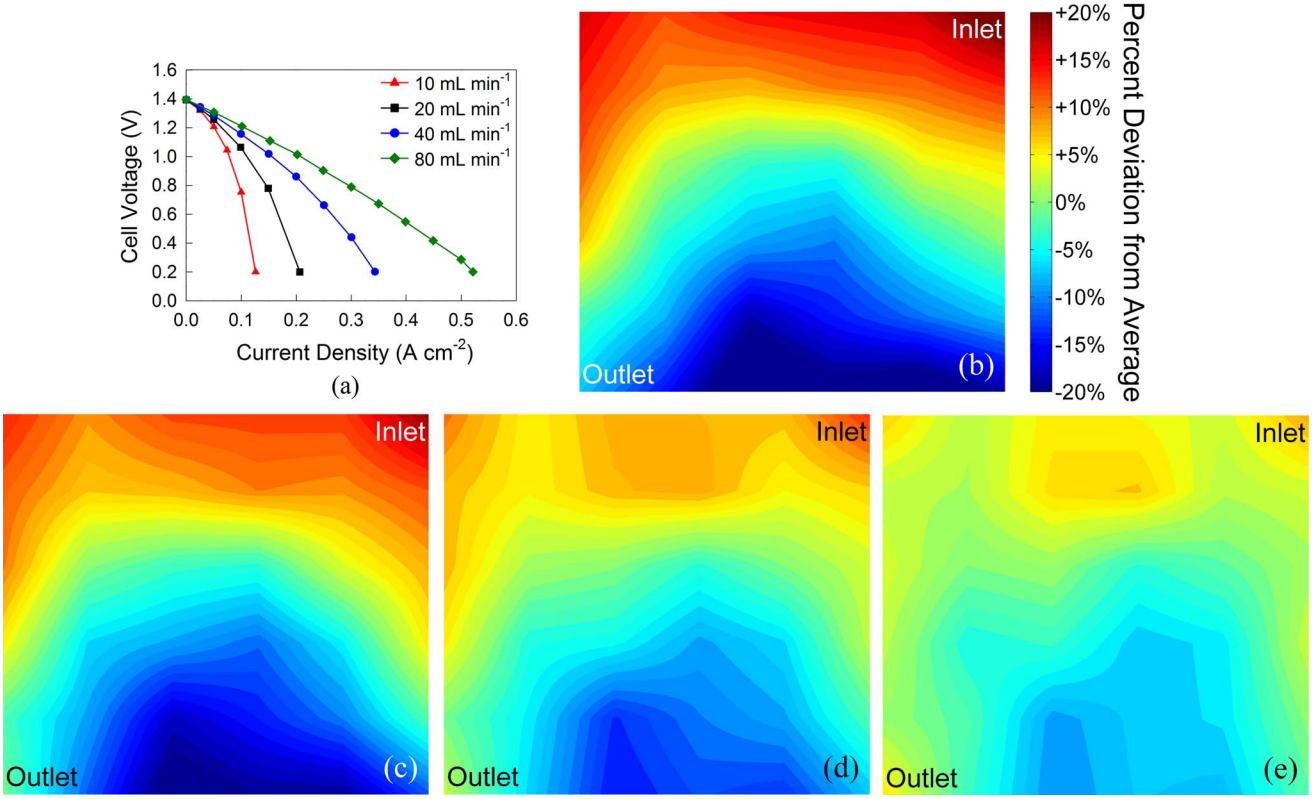

Figure 8. (a) Single-pass polarization curves at 25% SoC for different flow rates and corresponding current distributions at 0.2 V hold for (b) 10 mL min^{-1} (c) 20 mL min^{-1} (d) 40 mL min^{-1} (e) 80 mL min^{-1}.

density of 5 mA cm^{-2} with 95% SoC electrolyte at a flow rate of 5 mL min^{-1}.

Charging is not mass transport limited at moderately low current densities but this isn't necessarily the case for discharging. Since distributions reflect mass transport within the cell, these limitations can be induced at a low current density by altering operating parameters. Flow rate is a controllable parameter that impacts mass transport, as Figure 8 depicts with a comparison of performance and limiting current distribution as a function of flow rate. Figure 8a shows single-pass polarization curves at 25% SoC for the same cell build at four different flow rates. Figures 8b–8e show the corresponding distributions under limiting current conditions at the end of the polarization curves during a 0.2 V hold. At a flow rate of 10 mL min^{-1} the polarization curve shows a nonlinear drop in voltage indicating considerable mass transport overpotential. This is supported by the corresponding limiting current distribution shown in Figure 8b. These large current gradients identify a significant mass transport limitation because the upper half of the electrode sustains a much higher current while the lower half is underutilized. A higher flow rate eliminates the mass transport limitation and allows the electrode to be utilized more effectively. Figure 8a shows that at 80 mL min^{-1}, the cell performs significantly better and the nearly linear polarization curve indicates that, at high currents, the cell is dominated by ohmic losses rather than mass transport. This observation is also supported by the current distributions; at 10 mL min^{-1} (Figure 8b), large current gradients show significant mass transport limitations whereas at 80 mL min^{-1} (Figure 8e), the distribution is similar to a non-mass transport limiting condition. It should be noted that for all conditions the cells were operating with excess reactants at a stoichiometry between 3.5 and 6.9.

Since distributions reflect mass transport within the cell once a desired current can no longer be maintained at a constant flow rate, differences between current distributions can be utilized to identify transport differences between various electrode materials. In order to compare current distributions between electrode materials it was important to determine appropriate operating conditions to use for comparison. For all comparison tests, single-pass polarization curves were performed with the same electrolyte flow rate and SoC. A comparison between materials at the same operating current would seem the most appropriate; however, performance can vary significantly between different electrode materials.[31] At a given current density, one electrode could be in a mass-transport dominated region of the polarization curve with large in-plane current gradients (i.e. point (e) or (f) of Figure 5a) while a different electrode material may be in a kinetic or ohmic-dominated region with a nearly uniform distribution (i.e. point (b), (c), or (d) of Figure 5a). In this case, since the distribution is a reflection of electrolyte mass transport and concentration, it is more appropriate to compare distributions at their respective mass-transport limiting current density. The current distributions will then appropriately highlight the mass transport differences between electrode materials.

Heat treated electrodes have been shown to have improved performance relative to untreated electrodes.[6,31] Performance enhancement has been attributed to surface area and surface chemistry; however it should also be attributed in part to transport. Figure 9 shows a comparison of untreated carbon paper and heat treated carbon paper under limiting current conditions. It is evident that the heat treated electrode produced larger gradients than the untreated material at a limiting current condition. This can be attributed to two properties of treated material: improved wettability and higher active surface area.[31] The improved wettability enhances transport to the electrode fibers, which leads to greater utilization of the electrode. Higher surface area of the treated electrode provides additional reaction sites to support more reaction near the inlet. This in turn causes the electrolyte SoC to deplete at a greater rate as it passes through the cell, causing the outlet half of the active area to see a lower SoC (and concomitantly, lower active species concentrations). These two material property aspects lead to a larger gradient generated with the treated material. It should be noted that the treated electrode does reach a higher limiting current;

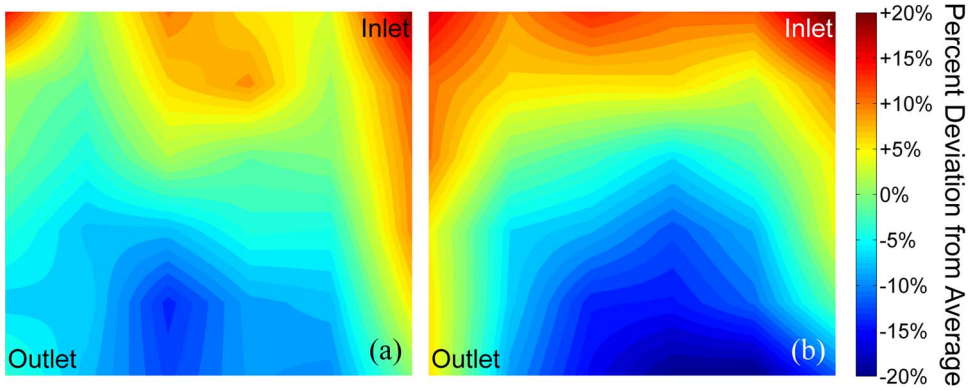

Figure 9. Effect of material properties on distribution from single-pass discharge polarization curves at limiting current density for 50% SoC electrolyte with (a) untreated carbon paper (300 mA cm^{-2}), and (b) heat treated carbon paper (350 mA cm^{-2}).

however, even at the limiting current density of an untreated electrode, it produced a larger current gradient (not shown).

Electrode treatment is one method of improving performance in these systems, however increasing the electrode thickness above that of a single layer of 10AA has also been shown to improve performance.[30] This enhanced performance can then change the shape of the polarization curve such that it is a nearly linear voltage-current relationship out to its limiting current. This indicates that the cell is dominated by ohmic losses and the resultant distributions shouldn't reflect any mass transport limitations in the cell. In order to ensure that this mass transport limitation was reached with thicker electrode builds, it was necessary to reduce the electrolyte SoC to 25% for the single-pass polarization curves.

In addition to performance change with additional electrode layers, the distribution also changes. A comparison of distributions at limiting current for a single layer, 3 layers, and 8 layers of untreated carbon paper electrodes are shown in Figure 10. Since the distribution reflects internal electrolyte velocity and reactive species concentrations, one would expect both parameters to influence the distribution. However, with a serpentine flow channel design, electrolyte velocity through the electrode doesn't change appreciably with increased electrode thickness.[25] Thus, the distribution change can be predominantly attributed to local electrolyte concentration. The extra electrode thickness provides additional active area for reaction and pathways for electrolyte transport. These two aspects allow more high-concentration electrolyte to enter the electrode near the top (inlet) of the active area and react before it is transported through the electrode at the channel switchbacks along the sides of the flow field.[25] However it is interesting that, although less pronounced, the characteristic high current down the sides is still noticeable with the addition of extra layers. In addition, since more reaction takes place toward the top of the active area, less current flows through the bottom half of the electrode, thus resulting in larger in-plane current gradients.

It should be noted that with a thicker electrode there is an increased chance for lateral current spread through the electrode. However, the fact that these gradients develop and are well-pronounced indicates that lateral spread is not significant. If lateral spread was a significant issue, the distribution would be more uniform across the active area. In addition, the distribution still displays the characteristic concave down shape with high current along the sides of the active area, which reflects mass transport characteristics for this pairing of flow field and electrode material.

Different electrode materials can also illustrate how material properties can impact distribution. A comparison of three different electrodes is presented in Figure 11: eight layers of carbon paper (nominal uncompressed thickness of 3.12 mm) and a single layer of carbon felt (uncompressed 3 mm) under two different compressions. A distribution comparison at limiting current between the eight layers of carbon paper and a single layer of carbon felt, both compressed to 75% of their original thickness, is shown in Figures 11a and 11b, respectively. The comparable thickness of these two electrode materials eliminates any electrode thickness influence on distribution. The carbon felt distribution displays much of the same characteristics of a thicker electrode as previously discussed: a nearly uniform distribution across the width of the distribution and smooth gradient from inlet (top) to outlet (bottom). However, one subtle difference exists when comparing the sides of the active area: the gradient is concave down at the outlet for the carbon paper whereas the felt displays a uniform gradient across the entire width. Since thickness is consistent between the two materials, this difference can be attributed predominantly to the physical properties of the material, namely porosity (summarized in Table I).

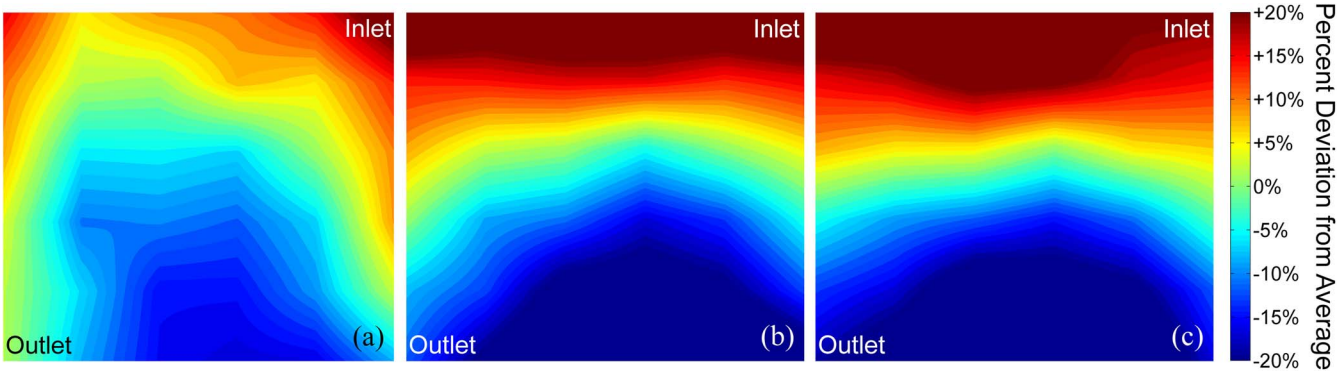

Figure 10. Effect of number of layers of untreated 10AA carbon paper on distribution at limiting current for 25% SoC electrolyte with (a) 1 layer (200 mA cm^{-2}), (b) 3 layers (300 mA cm^{-2}), (c) 8 layers (350 mA cm^{-2}).

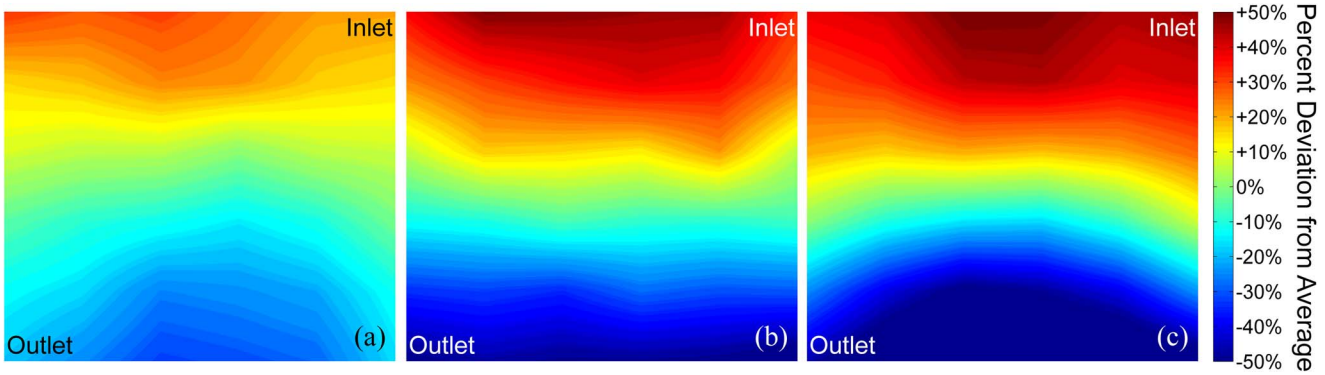

Figure 11. Effect of material properties on limiting current distribution at 25% SoC for (a) 8 layers of untreated carbon paper (350 mA cm^{-2}), (b) 1 layer of carbon felt compressed to 75% of its original thickness (400 mA cm^{-2}), (c) 1 layer of carbon felt compressed to 25% of its original thickness (450 mA cm^{-2}).

Table I. Porosity values for original and compressed carbon paper and carbon felt.[34–37]

Material	Compression	Porosity
10AA	None	84.7%[34]
10AA	75% original	79.6%
GFD3	None	94%[35,36]
GFD3	75% original	92%
GFD3	25% original	76%

To support the claim that porosity influences distribution, a carbon felt electrode was tested under extreme compression, to 25% of its original thickness. Under this compression, the felt has a comparable porosity to compressed carbon paper as shown in Table I. The resulting distribution comparison between the two compressions is shown in Figures 11b and 11c, where it is evident that the over-compressed felt displays the concave down gradient shape at the outlet, similar to that of carbon paper (Figure 11a). This indicates that reduced porosity enables more electrolyte transport to bypass the channels into the electrode along the sides of the active area, which is the path of least resistance.[25] It should be noted that the over-compressed felt was presumed to have deflected quite significantly into the flow channel as pressure drop was an order of magnitude higher for the over-compressed felt compared to regular compression. Regardless, it is evident that through material selection, thickness, and compression, the transport of these systems can be tailored to approach the desired distribution of uniform current across the active area.

Conclusions

The printed circuit board approach was successfully implemented to measure in-plane, two-dimensional localized current distribution in real-time in an operating VRFB. The PCB approach allows for higher spatial resolution and provides more flexibility in implementation of different flow field designs compared to other measurement techniques. A fully-segmented flow field plate is necessary to eliminate lateral current spread and ensure the measurement accurately reflects the distribution in the electrode.

It was demonstrated that the observed distribution reflects a combination of local electrolyte velocity in the electrode and electrolyte concentration. These aspects are especially prevalent once a mass-transport limiting condition is reached. Current distribution measurements during constant current charging reveal that charging is not typically a mass-transport limited process, but rather is limited by the electrochemical operating window of the all-vanadium redox couple. During constant current discharge processes, however, mass-transport limiting conditions identify inherent limitations with different electrode materials and material properties. Flow rate, electrode thickness, wettability, and porosity were all shown to impact distribution. These properties can be tailored to engineer a better electrode with improved electrode utilization and cell efficiency.

Acknowledgments

The authors acknowledge the Tennessee Solar Conversion and Storage using Outreach, Research, and Education (TN-SCORE) program (NSF EPS #1004083) for support. We would also like to acknowledge Rob Reid and Jon Owejan (formerly of General Motors) for their assistance with the design and implementation of this technique.

References

1. A. Z. Weber, M. M. Mench, J. P. Meyers, P. N. Ross, J. T. Gostick, and Q. Liu, *J. Appl. Electrochem.*, **41**, 1137 (2011).
2. M. Skyllas-Kazacos, M. H. Chakrabarti, S. A. Hajimolana, F. S. Mjalli, and M. Saleem, *J. Electrochem. Soc.*, **158**, R55 (2011).
3. C. Ponce de León, A. Frías-Ferrer, J. González-García, D. A. Szánto, and F. C. Walsh, *J. Power Sources*, **160**, 716 (2006).
4. X. Li, H. Zhang, Z. Mai, H. Zhang, and I. Vankelecom, *Energy Environ. Sci.*, **4**, 1147 (2011).
5. D. Chen, M. A. Hickner, E. Agar, and E. C. Kumbur, *Electrochem. Commun.*, **26**, 37 (2013).
6. B. Sun and M. Skyllas-Kazacos, *Electrochim. Acta*, **37**, 1253 (1992).
7. W. Li, J. Liu, and C. Yan, *Carbon*, **49**, 3463 (2011).
8. G. Wang, J. Chen, X. Wang, J. Tian, H. Kang, X. Zhu, Y. Zhang, X. Liu, and R. Wang, *J. Energy Chem.*, **23**, 73 (2014).
9. M. Vijayakumar, W. Wang, Z. Nie, V. Sprenkle, and J. Hu, *J. Power Sources*, **241**, 173 (2013).
10. R. M. Darling and M. L. Perry, *J. Electrochem. Soc.*, **161**, A1381 (2014).
11. T. Jyothi Latha and S. Jayanti, *J. Appl. Electrochem.*, **44**, 995 (2014).
12. X. Ma, H. Zhang, C. Sun, Y. Zou, and T. Zhang, *J. Power Sources*, **203**, 153 (2012).
13. K. W. Knehr and E. C. Kumbur, *Electrochem. Commun.*, **23**, 76 (2012).
14. Q. Liu, A. Turhan, T. A. Zawodzinski, and M. M. Mench, *Chem. Commun.*, **49**, 6292 (2013).
15. J. T. Clement, T. A. Zawodzinski, and M. M. Mench, *ECS Trans.*, **58**, 9 (2014).
16. W.-Y. Hsieh, C.-H. Leu, C.-H. Wu, and Y.-S. Chen, *J. Power Sources*, **271**, 245 (2014).
17. L. C. Pérez, L. Brandão, J. M. Sousa, and A. Mendes, *Renew. Sustain. Energy Rev.*, **15**, 169 (2011).
18. Ch. Wieser, A. Helmbold, and E. Gülzow, *J. Appl. Electrochem.*, **30**, 803 (2000).
19. A. B. Geiger, R. Eckl, A. Wokaun, and G. G. Scherer, *J. Electrochem. Soc.*, **151**, A394 (2004).
20. M. Noponen, T. Mennola, M. Mikkola, T. Hottinen, and P. Lund, *J. Power Sources*, **106**, 304 (2002).
21. M. M. Mench and C.-Y. Wang, *J. Electrochem. Soc.*, **150**, A79 (2003).
22. S. J. C. Cleghorn, C. R. Derouin, M. S. Wilson, and S. Gottesfeld, *J. Appl. Electrochem.*, **28**, 663 (1998).
23. J. J. Gagliardo, J. P. Owejan, T. A. Trabold, and T. W. Tighe, *Nucl. Instruments Methods Phys. Res. Sect. A Accel. Spectrometers, Detect. Assoc. Equip.*, **605**, 115 (2009).
24. D. S. Aaron, Q. Liu, Z. Tang, G. M. Grim, A. B. Papandrew, A. Turhan, T. A. Zawodzinski, and M. M. Mench, *J. Power Sources*, **206**, 450 (2012).
25. J. R. Houser, J. T. Clement, A. M. Pezeshki, and M. M. Mench, *J. Power Sources*, **302**, 369 (2016).
26. R. Eckl, R. Grinzinger, and W. Lehnert, *J. Power Sources*, **154**, 171 (2006).

27. I. A. Schneider, H. Kuhn, A. Wokaun, and G. G. Scherer, *J. Electrochem. Soc.*, **152**, A2092 (2005).
28. D. G. Strickland, S. Litster, and J. G. Santiago, *J. Power Sources*, **174**, 272 (2007).
29. F. T. Wandschneider, S. Röhm, P. Fischer, K. Pinkwart, J. Tübke, and H. Nirschl, *J. Power Sources*, **261**, 64 (2014).
30. Q. Liu, G. M. Grim, A. B. Papandrew, A. Turhan, T. A. Zawodzinski, and M. M. Mench, *J. Electrochem. Soc.*, **159**, A1246 (2012).
31. A. M. Pezeshki, J. T. Clement, G. M. Veith, T. A. Zawodzinski, and M. M. Mench, *J. Power Sources*, **294**, 333 (2015).
32. D. S. Aaron, Z. Tang, A. B. Papandrew, and T. A. Zawodzinski, *J. Appl. Electrochem.*, **41**, 1175 (2011).
33. H. Al-Fetlawi, A. A. Shah, and F. C. Walsh, *Electrochim. Acta*, **55**, 3192 (2010).
34. J. Hinebaugh, Z. Fishman, and A. Bazylak, *J. Electrochem. Soc.*, **157**, B1651 (2010).
35. SGL Carbon GmbH, *SIGRACET and SIGRACELL Components for Flow Batteries* (2012).
36. H. Zhou, H. Zhang, P. Zhao, and B. Yi, *Electrochim. Acta*, **51**, 6304 (2006).
37. M. M. Mench, *Fuel Cell Engines*, 1st ed., p. 528, John Wiley & Sons, Inc., (2008).